MNRAS 430, 2943–2950 (2013) doi:10.1093/mnras/stt097

Confirmation of the nature of the absorber in IRAS 09104+4109

Chia-Ying Chiang,[1]★ E. M. Cackett,[2] P. Gandhi[3] and A. C. Fabian[1]

[1]*Institute of Astronomy, University of Cambridge, Madingley Road, Cambridge CB3 0HA, UK*
[2]*Department of Physics and Astronomy, Wayne State University, 666 W. Hancock St, Detroit, MI 48201, USA*
[3]*Institute of Space and Astronautical Science, Japan Aerospace Exploration Agency, 3-1-1 Yoshinodai, chuo-ku, Sagamihara, Kanagawa 252-5210, Japan*

Accepted 2013 January 14. Received 2013 January 10; in original form 2012 November 22

ABSTRACT

We present the first long *Suzaku* observation of the hyperluminous infrared galaxy IRAS 09104+4109 which is dominated by a Type 2 AGN. The infrared to X-ray spectral energy distribution (SED) indicates that the source is an obscured quasar with a Compton-thin absorber. However, the 3σ hard X-ray detection of the source with the *BeppoSAX* PDS suggested a reflection-dominated, Compton-thick view. The high-energy detection was later found to be possibly contaminated by another Type 2 AGN, NGC 2785, which is only 17 arcmin away. Our new *Suzaku* observation offers simultaneous soft and hard X-ray coverage and excludes contamination from NGC 2785. We find that the hard X-ray component is not detected by the *Suzaku* Hard X-ray Detector/PIN (effective energy band 14–45 keV). Both reflection and transmission models have been tested on the latest *Suzaku* and *Chandra* data. The 0.5–10 keV spectrum can be well modelled by the two scenarios. In addition, our analysis implied that the absorption column required in both models is $N_{\rm H} \sim 5 \times 10^{23}$ cm^{-2}. Unless IRAS 09104+4109 is a 'changing-look' quasar, we confirm that it is a Compton-thin AGN. Although the lack of detection of X-ray emission above 10 keV seems to favour the transmission scenario, we found that the two models offer fairly similar flux predictions over the X-ray band below ~40 keV. We also found that the strong iron line shown in the *Suzaku* spectrum is in fact a blend of two emission lines, in which the 6.4 keV one is mostly contributed from the AGN and the 6.7 keV from the hot cluster gas. This implies that the neutral line is perhaps caused by disc reflection, and the reflection-dominated model is more likely the explanation. The transmission model should not be completely ruled out, but a deeper hard X-ray spectrum observation is needed to discriminate between the two scenarios.

Key words: accretion, accretion discs – quasars: individual: IRAS 09104+4109 – X-rays: galaxies.

1 INTRODUCTION

The hyperluminous infrared (IR) galaxy IRAS 09104+4109 ($z = 0.442$) hosted in a cD galaxy in a rich cluster (Kleinmann et al. 1988) is one of the most powerful (IR luminosity $>10^{46}$ erg s^{-1}) sources within $z = 0.5$. The active nucleus of IRAS 09104+4109 was classified as an obscured Type 2 quasar based on its optical spectrum characteristic (Kleinmann et al. 1988; Hines & Wills 1993; Tran, Cohen & Villar-Martin 2000), while the near-IR spectrum gave a consistent classification (Soifer et al. 1996). The *ASCA* observation showed that the source is bright in X-rays, with a power-law spectrum typically seen in most AGNs (Fabian et al. 1994). Hines & Wills (1993) analysed the VLA 1.4 and 5 GHz observations and found a double-lobed radio source with straight jets extending along north-west and south-east of the nucleus. The *ROSAT* High Resolution Imager observation revealed spatial extended X-ray emission with a central dip in the X-ray intensity (Fabian & Crawford 1995), which has been confirmed to be one of two cavities in north-west and south-east of the core with a new 76 ks *Chandra* observation (Hlavacek-Larrondo et al. 2012). O'Sullivan et al. (2012) presented new Giant Metrewave Radio Telescope (GMRT) observations and claimed that these X-ray cavities coincide with the radio jets, while Hlavacek-Larrondo et al. (2012) indicated that the cavities are coincident with hotspots. The peaked X-ray surface brightness profile resolved by *ROSAT* implied that the cluster has a strong cool core (Fabian & Crawford 1995; Crawford & Vanderriest 1996).

A strong emission line, probably associated with the reflection from a helium-like ion, was discovered in the *ASCA* spectrum. The similar fluxes found in *ASCA* (extrapolated) and *ROSAT* observations imply that the 0.1–10.0 keV X-ray emission is also likely contributed by the hot gas in the cluster, though the strong

★E-mail: cychiang@ast.cam.ac.uk

iron line might come from a hidden nucleus. Franceschini et al. (2000) reported a 3σ detection of a transmitted component above 10 keV by the *BeppoSAX* PDS. which indicated that the spectrum should be interpreted as a reflection continuum absorbed by a Compton-thick absorber. The equivalent width (EW) of the strong iron line given by the 9.1 ks *Chandra* observation (Iwasawa. Fabian & Ettori 2001) is ∼1–2 keV. which further supports the reflection-dominated scenario. However. the limited 0.1–10.0 keV X-ray spectra are not sufficient in distinguishing the transmission- and the reflection-dominated models. Piconcelli et al. (2007) analysed the 14 ks *XMM–Newton* observation and found no significant preference to these models. They indicated a possibility of 'contamination' from nearby sources, as the field of view of the PDS instrument of *BeppoSAX* is large ($1^{\circ} \times 1^{\circ}$). Also, the 2–10 keV luminosity measured by the transmission-dominated model is consistent with the expected value on the basis of the bolometric luminosity. The absorber along the line of sight of the nucleus of IRAS 09104+4109 is either Compton-thin or changed from Compton-thick to Compton-thin between the *BeppoSAX* and *XMM–Newton* observations in five years.

Vignali et al. (2011) found that both *Chandra* and optical/mid-IR spectral analysis imply heavy but not Compton-thick obscuration (i.e. that $N_{\rm H} > 10^{24}$ cm^{-2}). Moreover, they presented a 54-month *Swift* Burst Alert Telescope (BAT) map (15.0–30.0 keV band) which shows that the hard X-ray emission detected by *BeppoSAX* is probably associated with a $z = 0.009$ Type 2 AGN NGC 2785, which is only 17 arcmin away from IRAS 09104+4109. In order to investigate the ambiguous detection by *BeppoSAX* above 10 keV in depth. data from the hard X-ray band. where *XMM–Newton* and *Chandra* have no coverage. are necessary.

The recent observation with *Suzaku* offers simultaneous X-ray data of 0.5–10.0 and 14.0–45.0 keV of the source. Given that the fields of view of *Suzaku* X-ray Imaging Spectrometer (XIS) and PIN are 17.8 arcmin × 17.8 arcmin and 34 arcmin × 34 arcmin. respectively, emission from the nearby AGN NGC 2785 is likely included in the PIN detector if the pointing is aimed at IRAS 09104+4109 (RA. Dec. $= 09^{\rm h}13^{\rm m}45\overset{\rm s}{.}49, 40^{\circ}56'28\overset{''}{.}2$). The *Suzaku* PIN is a non-imaging instrument and emission from other sources cannot be simply excluded by region extraction. Therefore, we shifted the pointing 6 arcmin west (new RA. Dec. $= 09^{\rm h}13^{\rm m}21\overset{\rm s}{.}49, 40^{\circ}56'28\overset{''}{.}2$) and assigned a 90° roll angle in our observation. The entire source still lies within the XIS detector after the change of pointing, and contribution from NGC 2785 should be excluded from the field of view of PIN.

Once the hard X-ray detection of IRAS 09104+4109 by the *BeppoSAX* PDS is also seen by the *Suzaku* PIN. it would confirm the reflection-dominated picture. Compton-thick AGNs are important in understanding the evolution of supermassive black holes. So far, these objects are mostly found at low redshifts ($z < 0.05$; Comastri 2004). If IRAS 09104+4109 is Compton-thick, it will be one of the few distant Compton-thick AGNs to have reliable X-ray spectroscopic data. A relatively few such objects are known at the moment. Luminous Compton-thick AGNs with well-studied multi-wavelength data are useful for understanding an important evolutionary phase in the growth of supermassive black holes.

This paper presents an analysis for the first *Suzaku* long observation of IRAS 09104+4109 and offers conclusive results about the nature of the absorber in the source. It has been debated for years that the X-ray spectrum is transmission or reflection dominated. and we will discuss this in detail in Section 4. Calculations in this paper were assumed a flat cosmology with $H_0 = 71$ km s^{-1} Mpc^{-1}, $\Omega_\lambda = 0.73$ and $\Omega_0 = 0.27$.

2 DATA REDUCTION

2.1 *Suzaku*

IRAS 09104+4109 was observed with *Suzaku* during 2011 November 18–20 resulting in a total of ∼113 ks of good exposure time. The XIS was operated in the normal mode. and both 3 × 3 and 5 × 5 editing modes were operated in all detectors (XIS0. XIS1 and XIS3). As mentioned in the previous section. the pointing has been shifted by 6 arcmin. The source still lies perfectly within the XIS field of view. and no other point sources can be seen. Data have been reduced using the HEASOFT v6.11.1 software package with the latest calibration data base following the standard procedure. The source spectrum was extracted using XSELECT from a circular region with a radius of 110 arcsec. A larger circular region with a 180 arcsec radius has been used for background estimation from a source-free region. Response files were produced by the script XISRESP, which calls XISRMFGEN and XISSIMARFGEN to generate redistribution matrix files (RMF) and ancillary response files (ARF). respectively. We combined spectra and response files of the two front-illuminated (FI) CCD XIS detectors (XIS0 and XIS3) using the script ADDASCASPEC in FTOOL. The spectral bins of all spectra were grouped for at least 20 counts. We use the FI spectrum over 0.5–10.0 keV. and the back-illuminated (BI) spectrum over 0.5–7.0 keV for further analysis, as the signal-to-noise ratio of the BI data is lower at high energies.

The Hard X-ray Detector (HXD) was operated in XIS nominal pointing mode. A non-X-ray background (NXB) and a cosmic X-ray background (CXB) should be combined to form the total HXD/PIN background spectrum. We obtained the NXB event file directly from the *Suzaku* Data Centre and extracted it using the background model D (the tuned model). The CXB was simulated using the PIN response for a flat emission distribution. The count rate of source before background correction is 0.340 ± 0.002 counts s^{-1} in the effective PIN energy band 14.0–45.0 keV (all the count rates of PIN will be given over this band if not specified), appearing below the total background level (0.343 ± 0.001 counts s^{-1}). As the count rates of the source and the background are at a similar level (see also the upper panel in Fig. 1), we produced the earth-occulted

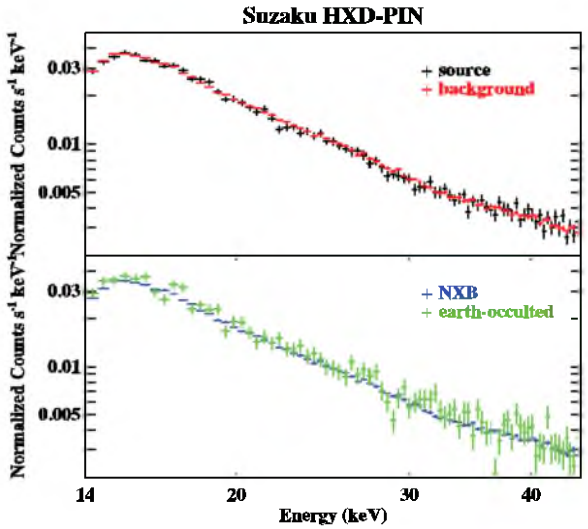

Figure 1. The upper panel shows the PIN data (before background correction) in black points and the total background in red points. The lower panel compares the NXB and the earth-occulted background, which are shown in blue and green points, respectively.

background for a further check. The earth-occulted background is ideally consistent with the NXB. and it should replace the NXB if discrepant. The lower panel in Fig. 1 shows that the earth-occulted background (green data points) and the NXB (blue points) are in good agreement. The count rate of the earth-occulted background (0.344 ± 0.004 counts s^{-1}) is slightly higher than that of the NXB (0.325 ± 0.001 counts s^{-1}), confirming the non-detection in the PIN band. Thus, we do not include the PIN spectrum in all our spectral fittings. Although the hard X-ray emission from IRAS 09104+4109 is beyond detection in the HXD/PIN. we can estimate an upper limit of flux by including the systematic error of the NXB and CXB. We generated an ARF for the HXD/PIN using the HXDARFGEN tool. The output ARF was coupled with the 'hxdnominal' response file 'ae_hxd_pinhxnome11_20110601.rsp' to account for the off-axis correction. The resulting 14.0–45.0 keV fluxes of the NXB and CXB are around 2.16×10^{-10} and 9.23×10^{-12} erg cm^{-2} s^{-1}. Considering the systematic error of the NXB to be 3 per cent (for observations with more than 10 ks exposure time[1]) the lower limit of the total background flux can be calculated. The background-uncorrected 14.0–45.0 keV flux of the source is $\sim 2.23 \times 10^{-10}$ erg cm^{-2} s^{-1}, and we hence estimate the upper limit of the background-corrected source flux to be $\sim 4.25 \times 10^{-12}$ erg cm^{-2} s^{-1}. The observed *BeppoSAX* PDS 20–100 keV flux is $\simeq 10^{-11}$ erg cm^{-2} s^{-1}, which is higher than the PIN upper limit $\sim 6.26 \times 10^{-12}$ erg cm^{-2} s^{-1} in the same band.

2.2 *Chandra*

The *Chandra* Advanced CCD Imaging Spectrometer (ACIS) observed IRAS 09104+4109 on 2009 January 6 for about 76 ks in very faint mode. We used tools in the latest CIAO v4.4 software package to reduce the data. The observation ends up with a good exposure of ~72 ks after background flare filtering. The nucleus of the cluster appears as a point source in the 0.5–7.0 keV (effective energy band of the ACIS) image. Since IRAS 09104+4109 is a strong cool-core cluster showing a significant radial temperature gradient, background subtraction could be critical in some circumstances. Thanks to the excellent point spread function of the *Chandra* ACIS, the nucleus spectrum can be extracted from a circular region with a 1 arcsec radius. In this case, the background was extracted from the surrounding 2–4 arcsec annulus in order to avoid possible source emission outside the 1 arcsec radius region and collect enough counts for the chi-statistics. The resulting spectrum contains emission from the nucleus of the cluster. and has excluded the thermal contribution from nearby hot gas. We also generated a spectrum with a 55 arcsec radius source region and a 55–110 arcsec annulus background region for comparison to our *Suzaku* data (regions used in the *Suzaku* observation are too large and would include edges of the chips of the ACIS). All the point sources resolved by *Chandra* within the background region have been removed for clean background extraction. Finally, we grouped both of our *Chandra* spectra with a minimum of 20 counts per bin as we did for the *Suzaku* data.

The *Chandra* spectra obtained by different reduction strategies are shown in Fig. 2. There seems to be a drop between the <2 keV and the >3 keV bands in the nucleus spectrum, but it is not obvious in the spectrum extracted from the 55 arcsec radius region (hereafter the *Chandra* 55 arcsec spectrum). We also plotted both the *Suzaku* FI XIS and BI XIS spectra in Fig. 2. The shape of the

[1] http://heasarc.gsfc.nasa.gov/docs/suzaku/prop_tools/suzaku_td/

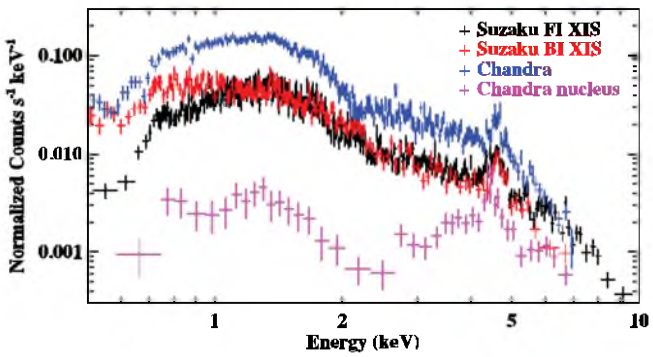

Figure 2. The spectra we extracted from both *Suzaku* and *Chandra* Observations. The data points have been mildly re-binned for clarity. The differences below ~1 keV between the *Suzaku* FI and BI XIS spectra are due to different calibrations. We ignore the *Suzaku* BI XIS data above 7 keV due to a poor signal-to-noise ratio.

Suzaku FI XIS spectrum is fairly similar to that of the *Chandra* 55 arcsec spectrum. which is expected because they were both extracted from a region including the nucleus and nearby hot gas. The flux difference between them is likely due to different background subtraction areas. A clear redshifted iron line appears in all spectra. Interestingly, the iron line in the *Chandra* nucleus spectrum seems to peak at a different energy from that of the 55 arcsec and *Suzaku* spectra. This will be further investigated in the following section.

3 DATA ANALYSIS AND COMPARISON

3.1 Iron line

A strong iron line with EW ~ 300–1200 eV (e.g. Franceschini et al. 2000; Iwasawa et al. 2001; Piconcelli et al. 2007) has been reported in all previous X-ray studies of this source. The EW is a model-dependent quantity, causing differences in values quoted in the previous literature. We first fitted a simple model composed of a power law and a Gaussian line to the 3.0–7.0 keV band of our data. The rest line energy of the *Suzaku* spectra is $6.63^{+0.03}_{-0.04}$ keV. consistent with the value 6.64 ± 0.05 keV given by the *Chandra* 55 arcsec spectrum. Nevertheless, the rest line energy of the iron line in the *Chandra* nucleus spectrum is 6.42 ± 0.06 keV instead of ~6.6 keV found in other spectra. We plot the data/model (fitted with a power law only) ratio of the *Chandra* data in Fig. 3, in which the different peaks of the line can be seen. As the *Chandra* 55 arcsec and *Suzaku* spectra also include emission from the nucleus, the iron

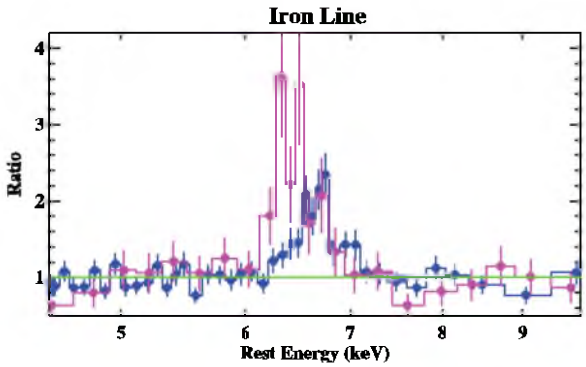

Figure 3. The data/model ratio of the *Chandra* nucleus (magenta points) and 55 arcsec (blue points) spectra, which have been fitted with a simple power law. It can be seen that the line energies are different.

Table 1. Fitting parameters that are bound in all data. $N_{\rm H}$ in this table shows the absorption column of *zphabs*. Γ is the photon index of the power-law component. kT_1 and kT_2 are the temperatures of the two thermal plasma components. Errors have been calculated at the 90 per cent confidence level.

Model	$N_{\rm H}(10^{22}\ {\rm cm}^{-2})$	Γ	kT_1 (keV)	kT_2 (keV)	$Z/Z_\odot$	χ^2/d.o.f.
Reflection	$45.3^{+22.9}_{-12.0}$	$1.59^{+0.31}_{-0.19}$	$2.22^{+1.16}_{-0.43}$	$6.36^{+1.64}_{-0.90}$	$0.42^{+0.07}_{-0.06}$	1065.5/1152
Transmission	$53.5^{+23.0}_{-21.6}$	$1.28^{+0.63}_{-0.65}$	$3.25^{+1.18}_{-1.23}$	$7.03^{+2.97}_{-1.67}$	$0.68^{+0.17}_{-0.12}$	1072.4/1150

line shown in these spectra should be formed by two components, in which one of them is attributed to the nucleus and the other to the diffuse hot gas. In most literature to date, the iron line shown in the X-ray spectra of IRAS 09104+4109 has been treated as a single line instead of two. It is not surprising that the line energy and EW of the iron line obtained from different data sets are in disagreement. Vignali et al. (2011) also suggested the possibility that the iron emission line is originated by a blend of emission features from both the central AGN and cluster gas.

We hereafter decomposed the iron line shown in the *Chandra* 55 arcsec spectrum into two Gaussian components and re-fitted the data. The rest line energy of the second Gaussian component turned out to be $6.70^{+0.05}_{-0.10}$ keV. The EWs obtained for both iron line components are 82^{+50}_{-37} eV for the 6.42 keV line, and 227^{+173}_{-81} eV for the 6.70 keV line, respectively. As for *Suzaku* data, the EWs are 87^{+45}_{-39} eV for the 6.42 keV line and 260^{+115}_{-99} eV for the 6.70 keV line. which are consistent with the *Chandra* 55 arcsec spectrum. The EW found in the *Chandra* nucleus spectrum is high (EW $= 338^{+152}_{-133}$ eV) possibly owing to a lower continuum level. Although in Fig. 3 it seems that the lines in both spectra are of similar line widths, the line shown in the nucleus spectrum can be fitted by a narrow (line width <0.1 keV) Gaussian line and no further components are required. In the following analysis, we model the iron line in the 55 arcsec and *Suzaku* spectra with two decomposed line components.

3.2 Spectral fitting

We started a detailed spectral analysis by constructing a model to explain the *Chandra* nucleus spectrum. The origin of the 6.42 keV Fe K line is generally attributed to reflected emission from cold matter illuminated by high-energy photons. Hence, a neutral reflection continuum might be needed in the model. In addition, the structures in the hard (>3 keV) and soft (<2 keV) energy bands in the *Chandra* nucleus spectrum shown in Fig. 2 seem to be symmetric, implying that the <2 keV component can be the redshifted Fe-L complex caused by strong reflection. Iwasawa et al. (2001) also suggested this possibility in their analysis of the ~9 ks *Chandra* observation. We fit a model composed of an absorbed power-law component *powerlaw* and a reflection continuum *reflionx* (Ross & Fabian 2005) in XSPEC to the *Chandra* nucleus spectrum. The photon index in the *reflionx* component has been set identical with that in the *powerlaw* component, and allowed to vary in a range between 1.4 and 3.3 which is reasonable for the reflection scenario. The ionization parameter ξ in *reflionx* was set to unity ($\xi = 1.0$) to model the 6.4 keV Fe K emission line from a neutral reflector with solar abundance. The Galactic absorption column $N_{\rm H} = 1.8 \times 10^{20}$ cm^{-2} (Murphy et al. 1996) is also included and modelled by TBNEW[2] (Wilms et al., in preparation) with the Wilms abundance. The absorption component in the source has been modelled using ZPHABS. Nevertheless, the model cannot, even with a high iron abundance, explain the low-energy excess in the spectrum well. It seems more likely that the low-energy hump in the core-only spectrum is caused by photoionized gas. We added a thermal plasma component *mekal* (Mewe, Gronenschild & van den Oord 1985; Liedahl, Osterheld & Goldstein 1995; see also Kaastra 1992) which includes line emission from several elements and the Fe-L complex to the model and obtained a better fit.

In order to extend the model to a version that can explain the *Chandra* 55 arcsec and *Suzaku* spectra, the 6.7 keV Fe XXV emission line shown in these spectra should be modelled. If the line originates from reflection, it should come from part of a highly ionized accretion disc which is usually close to the central black hole, where the illuminating source is nearby. By comparing the *Chandra* spectra extracted from different source regions, it is obvious that the 6.7 keV line is generated from the environment around the nucleus but not the central AGN. In addition, the X-ray emitting region of a typical AGN is expected to be small, and a spectrum extracted from 2–4 arcsec, which corresponds to ~20–30 kpc, should contain no X-ray emission from the nucleus of AGN. Hence, the 6.7 keV is more likely scattered by the hot diffuse gas instead of reflected from the accretion disc. We then added another *mekal* component with a high gas temperature into the model to fit the 6.7 keV line. The resulting full model can be expressed as *tbnew**(*zphabs***powerlaw* + *reflionx* + $mekal_1$ + $mekal_2$). We set the normalization of $mekal_2$ to be 0 for the *Chandra* nucleus spectrum, as this component is not required here. The *Chandra* and *Suzaku* observations differ by about 2 yr, which is short for a quasar to evolve dramatically. We expected the *Chandra* and *Suzaku* data to be slightly different in flux only. The main variables in the model, that are, the absorption column $N_{\rm H}$ of *zphabs*, the photon index Γ, and the temperature kT and the metallicity $Z/Z_\odot$ in the *mekal* component, are bound in all data sets. We assume that there is only an instrumental cross-calibration constant between the *Chandra* 55 arcsec spectrum and *Suzaku* data, and bind normalizations of all model components together. As for the *Chandra* nucleus spectrum, normalizations of the power-law component, the *reflionx* component and the $mekal_1$ component are allowed to vary in a way different from the other spectra. We summarized the fitting parameters of the reflection model in Table 1, and normalizations of parameters in Table 2.

The reflection model we constructed is similar to the 'absorbed powerlaw + *mekal* + reflection' model used in Franceschini et al. (2000). However, in their work an absorption column greater than 5×10^{24} cm^{-2} is required, while in Table 1 it can be clearly seen that the absorption column required here is $N_{\rm H} \sim 4.5 \times 10^{23}$ cm^{-2}, which is heavy but Compton-thin. The value is consistent with the number suggested by the transmission scenario ($N_{\rm H} \sim 5 \times 10^{23}$ cm^{-2}; Piconcelli et al. 2007; Vignali et al. 2011). Since the HXD/PIN has no solid detection in the high-energy band, the transmission model is a plausible explanation as well. We constructed a transmission

[2] http://pulsar.sternwarte.uni-erlangen.de/wilms/research/tbabs/

Table 2. The fitting parameters which have not been shown in Table 1. N_{pow}, N_{mek1}, N_{mek2} and N_{ref} represent the normalization of the power-law component, the two *mekal* components and the reflection component, respectively. F_{14-45} and F_{20-80} are the 14–45 and 20–80 keV fluxes predicted by the model. All fluxes are shown in erg cm^{-2} s^{-1}.

Parameter	*Suzaku* FI and BI	*Chandra* 55 arcsec	*Chandra* Nucleus
		Reflection	
N_{pow}	$7.9^{+10.0}_{-7.0} \times 10^{-5}$		$2.4^{+3.2}_{-1.3} \times 10^{-4}$
N_{mek1}	$8.1^{+9.9}_{-4.1} \times 10^{-4}$		$1.3^{+0.2}_{-0.3} \times 10^{-4}$
N_{mek2}	$2.7^{+0.4}_{-1.0} \times 10^{-3}$		0 (fixed)
N_{ref}	$3.3^{+2.0}_{-1.1} \times 10^{-5}$		$3.7^{+3.1}_{-1.7} \times 10^{-5}$
F_{14-45}	$^{*}2.37 \times 10^{-12}$	2.10×10^{-12}	3.20×10^{-12}
F_{20-80}	$^{*}2.89 \times 10^{-12}$	2.55×10^{-12}	4.18×10^{-12}
		Transmission	
N_{pow}	$9.5^{+27.5}_{-7.4} \times 10^{-5}$		$1.6^{+4.3}_{-1.1} \times 10^{-4}$
N_{mek1}	$1.5^{+1.6}_{-1.0} \times 10^{-3}$		$(1.4 \pm 0.2) \times 10^{-4}$
N_{mek2}	$2.0^{+1.0}_{-1.1} \times 10^{-3}$		0 (fixed)
F_{14-45}	$^{*}1.89 \times 10^{-12}$	1.68×10^{-12}	2.78×10^{-12}
F_{20-80}	$^{*}3.12 \times 10^{-12}$	2.76×10^{-12}	4.70×10^{-12}

*Since the predicted values for *Suzaku* XIS FI and BI spectra are fairly similar, we quoted that of the FI spectrum only.

model by replacing the *reflionx* component with a Gaussian line using *zgauss* in XSPEC. The constraint on the range of the photon indices has been lifted. Again we bind the main parameters in all data as we did when fitting with a reflection model. We allow normalizations of the power-law component, the $mekal_1$ component and the *zgauss* component in the *Chandra* nucleus spectrum to vary independently, while normalizations of these components in the other three spectra are bound together. The results have been again listed in Tables 1 and 2.

The transmission scenario also suggests a Compton-thin absorber with an absorption column of $\sim 5.4 \times 10^{23}$ cm^{-2}, which is consistent with that obtained by the reflection model and previous studies. Most of the resulting fitting parameters of both models are close and consistent at the 90 per cent confidence level. The photon index needed in each model is slightly different perhaps due to different broad-band continuum (see also Fig. 4). The same reason may cause the differences in the temperatures of *mekal* components. Because the *reflionx* generates emission features in the soft X-ray band ($\sim$1 keV) and the iron line band, temperatures required in the *mekal* components might be discrepant when the reflection continuum is replaced. The $mekal_1$ component is probably contributed by the thermal emission in the nucleus (the 1 arcsec radius circular region), and the $mekal_2$ originated from the hot gas in the region outside the nucleus. The gas temperature of $mekal_1$ we obtained by each model is below 4 keV, which is consistent with the results of O'Sullivan et al. (2012). Our fitting gives a gas temperature of $\sim$7 keV for $mekal_2$, which also lies well in the 5–8 keV range indicated by O'Sullivan et al. (2012). The values suggested by either the reflection or the transmission model are reasonable. As for the metallicity, values obtained by our models are close and only in mild disagreement. The best-fitting metallicity of the transmission model is closer to the value reported in O'Sullivan et al. (2012), but that implied by the reflection model still lies within their 1σ uncertainties.

The reflection and transmission models we tested in this data set result in comparable reduced χ^2 (see Table 1). Even with a better signal-to-noise ratio, X-ray data covered across the 0.5–10.0 keV band are not sufficient to distinguish these two interpretations. The lack of high-energy coverage makes model selection difficult, and the results are of no significant statistical difference. Fig. 4 shows the theoretical predictions from both models, and it can be clearly seen that they are fairly similar below 10 keV and start to divert above $\sim$40 keV. The hard X-ray fluxes, especially the 20–80 keV band, predicted by these models are fairly close (see Table 2) and both below the upper limit estimated in Section 2. As the results of the two models are statistically comparable, we will discuss in the following section the physical possibility of both models. The absorption-corrected rest-frame 2–10 keV luminosities (calculated from the numbers shown in Table 3) of the nucleus are $\sim(1.3\text{–}2.3) \times 10^{44}$ and $\sim(1.4\text{–}2.2) \times 10^{44}$ erg s^{-1}, predicted by the reflection and transmission models, respectively. These values are slightly higher than $(1.2\text{–}1.3) \times 10^{44}$ erg s^{-1} which was reported in Vignali et al. (2011), but lower than the predicted value of $\sim 10^{45}$ erg s^{-1} obtained by the same authors based upon IR observations from Lanzuisi et al. (2009). Using instead the mid-IR–X-ray correlation of local Seyferts from Gandhi et al. (2009) results in an upper limit to the X-ray power of $\sim 5 \times 10^{45}$ erg s^{-1}. This limit is consistent with the observations but several times higher, because of the fact that IR data on this source are from the *Spitzer* mission, which cannot spatially resolve the nucleus emission from stellar activity in typical ultra- and hyperluminous IR galaxies (see Gandhi et al. 2009; Vignali et al. 2011).

4 DISCUSSION

4.1 Nature of the absorber

The main supporting evidence of the Compton-thick interpretation is the hard X-ray detection by the *BeppoSAX* PDS instrument. In our latest *Suzaku* observation, the pointing has been shifted to avoid possible contamination from the nearby Type 2 AGN NGC 2785. As a result, the *Suzaku* HXD/PIN gave no solid detection but an estimated upper limit which is still lower than the measured *BeppoSAX* flux, and the marginal 3σ *BeppoSAX* detection is therefore questionable. The non-detection in the hard X-ray band also implies that the reflection model used in Franceschini et al. (2000) is not necessarily required to explain the data. The hard X-ray flux obtained by the *BeppoSAX* observation was so high that the extrapolated transmission model failed to reach the flux, and the only possibility was to attribute the high-energy transmitted component to inverse Compton scattering. In order to explain the broad-band X-ray data, the reflection continuum has to be heavily absorbed by extreme absorption column across the X-ray band below 10 keV and produce a Compton hump to interpret the hard X-ray emission. Piconcelli et al. (2007) and Vignali et al. (2011) obtained a similar high-energy flux prediction using a reflection continuum without absorber. They assumed that the absorber is of the same nature as the reflector, so using a reflection continuum automatically implies an optically thick ($\tau > 1$) absorber. However, considering that the broad iron line displayed in the *Suzaku* XIS spectrum is a blend of two emission lines which can be caused by different mechanisms, the reflection scenario should not be ruled out. The narrow 6.4 keV Fe K line could be reflected from the cold, optically thick accretion disc in the central AGN. In this case, it is not controversial to model the data with a reflection continuum, as the optically thick

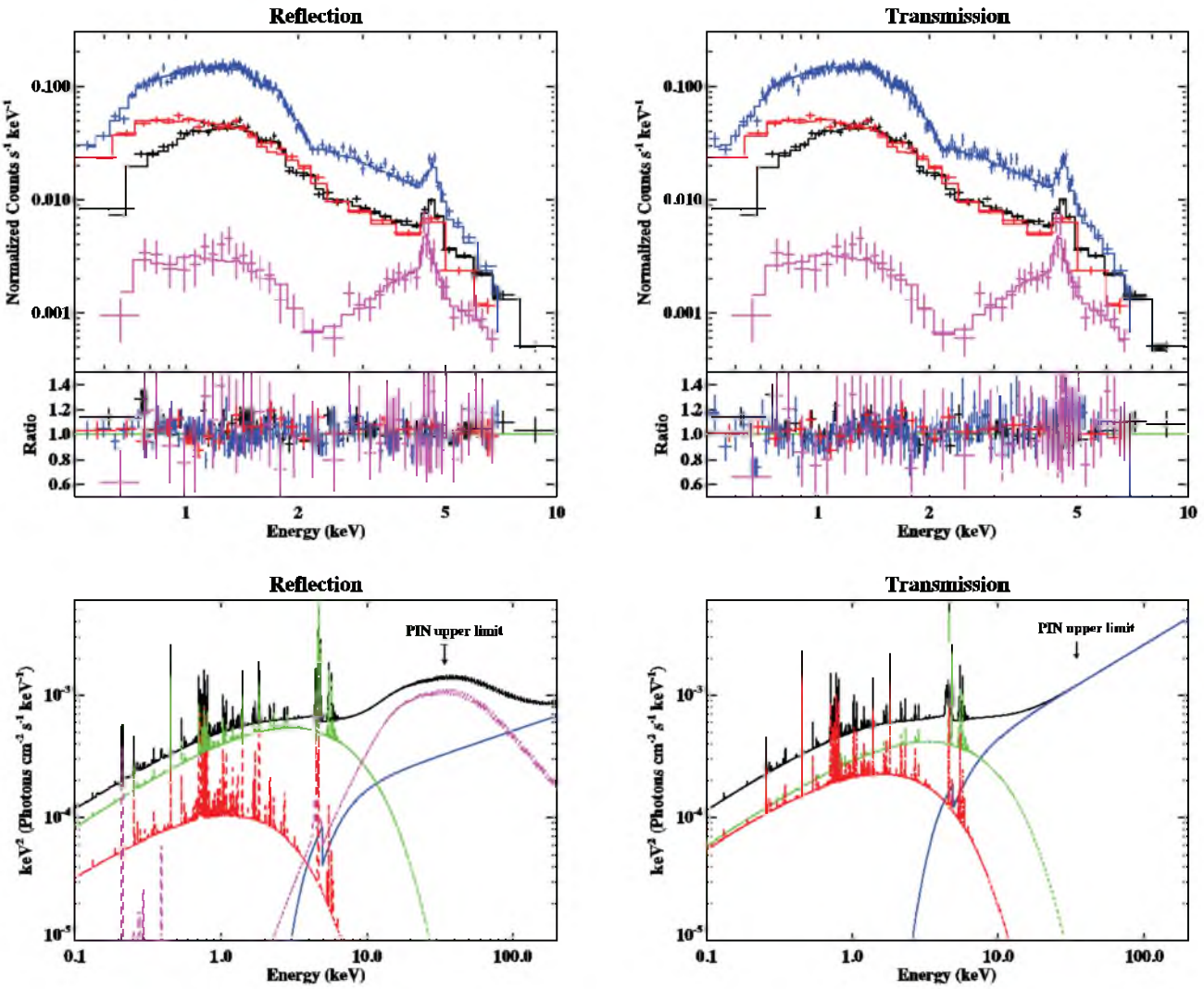

Figure 4. The upper set of figures shows the spectral fittings of the reflection and transmission models, while the lower set shows the decomposed components of the models. In the two upper plots, colours of each spectrum are expressed in the same way as in Fig. 2. In both lower figures, the black solid line is for the total model and the coloured ones represent contributions from different components. The green and red dot–dashed lines show the two *mekal* components of different temperatures. We plot the absorbed power law as a blue solid line in both panels, and the reflection component has been shown as a magenta dash line. The Galactic absorption has been taken out in these figures.

reflector could be part of the accretion disc and not necessarily act as an absorber. The reflection scenario is completely plausible here.

In our analysis, the absorption columns required in the reflection and transmission models are not extreme, and both scenarios give consistent values ($\sim 5 \times 10^{23}$ cm^{-2}). The absorption column is correlated with the photon index, and we plot a contour of these parameters. It can been seen in Fig. 5 that the absorption column spans a range of Compton-thin values when the photon index varies. In previous studies, the reflection model always links to a Compton-thick absorber, but we showed here that the reflection scenario does not necessarily imply the Compton-thick interpretation. As we mentioned before, the reflector needs not to be the absorber, and it is not surprising that we obtained a Compton-thin result using the *reflionx* model. If the *BeppoSAX* PDS detection is solid, the reflection model is the only interpretation capable of explaining the high-energy flux. Nevertheless, as the hard X-ray emission is weak, the reflection model can still explain the spectrum well. The key to determine the nature of absorber is the flux above 10 keV, but not

Table 3. The absorption-uncorrected rest frame 2–10 keV flux $^{*}F_{2-10}$, and the intrinsic 2–10 keV absorption-corrected flux F_{2-10}. $F_{\rm thermal}$ and $F_{\rm nucleus}$ are the decomposed components of F_{2-10} from thermal emission of the cluster gas and the nucleus. Fluxes are all shown in erg cm^{-2} s^{-1}.

Flux	*Suzaku* XIS	*Chandra* 55 arcsec	*Chandra* nucleus
		Reflection	
$F_{2-10}{}^{*}$	2.00×10^{-12}	1.76×10^{-12}	1.04×10^{-12}
F_{2-10}	1.74×10^{-12}	1.54×10^{-12}	3.53×10^{-13}
$F_{\rm thermal}$	1.53×10^{-12}	1.36×10^{-12}	2.28×10^{-14}
$F_{\rm nucleus}$	2.08×10^{-13}	1.84×10^{-13}	3.31×10^{-13}
		Transmission	
$F_{2-10}{}^{*}$	2.14×10^{-12}	1.89×10^{-12}	9.49×10^{-13}
F_{2-10}	1.74×10^{-12}	1.54×10^{-12}	3.53×10^{-13}
$F_{\rm thermal}$	1.52×10^{-12}	1.35×10^{-12}	3.77×10^{-14}
$F_{\rm nucleus}$	2.20×10^{-13}	1.95×10^{-13}	3.15×10^{-13}

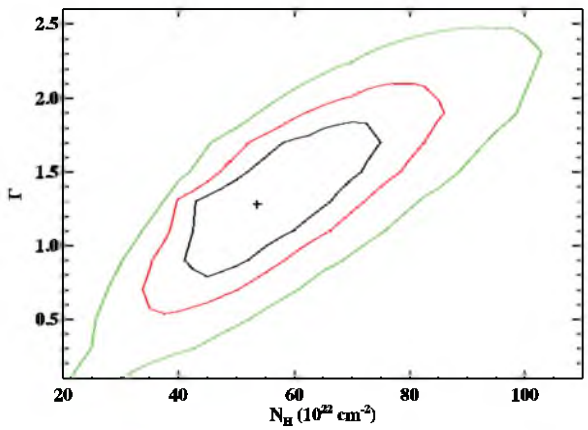

Figure 5. The contour plot of the column density of the absorber $N_{\rm H}$ against the photon index Γ. Contours are plotted at 67 (green), 90 (red) and 99 (black) per cent levels.

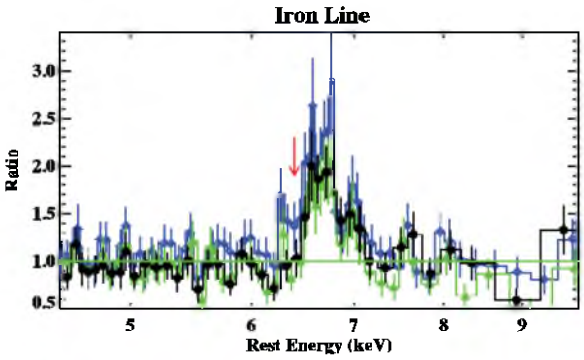

Figure 6. The data/model ratio of the *Chandra* 55 arcsec (blue open diamonds), the 2–55 arcsec (green triangles) and the 5–55 arcsec (black points) spectra, which have been fitted with a simple power law. The red arrow points to the energy of the 6.4 keV line.

the model used to fit the data. It has been debated for a while that whether the absorber is Compton-thick or not. Now our analysis gives a conclusive result that the absorber in IRAS 09104+4109 is Compton-thin. provided that it is not a 'changing-look' quasar.

4.2 Reflection or transmission above 10 keV

The two models we tested in this work gave statistically comparable results and similar fitting parameters. The predicted high-energy fluxes are both below the upper limit given by the HXD/PIN. We found that our predictions are also under the upper limit implied by the *Swift* BAT map (Vignali et al. 2011). The 3σ upper limit in the 15–30 keV band implied by the BAT map is $\sim 1.9 \times 10^{-12}$ erg cm^{-2} s^{-1}, and the predicted fluxes in this band are (1.2–1.8) $\times$ 10^{-12} and (8.8–14.3) $\times$ 10^{-13} erg cm^{-2} s^{-1} for the reflection and transmission models, respectively. The reflection scenario has been ruled out in some studies due to its high-flux prediction across the hard X-ray band. In our study, the reflection model works as well as the transmission model while no hard X-ray detection has been confirmed. The lack of high-energy emission does not automatically imply that the reflection model is out of consideration. Piconcelli et al. (2007) indicated that the source does not display an iron line with a high enough EW expected for a truly reflection-dominated spectrum. Nonetheless, in the reflection scenario a reflection spectrum does not necessarily come along with a strong iron line, as it is not the only feature produced by reflection. For instance, the Compton hump and soft excess are signatures of reflection as well (though the soft X-ray band of IRAS 09104+4109 is dominated by thermal emission from the cluster gas). In a case that the iron abundance is not high, the EW of the iron line can be low but the Compton hump is present. Thus, the EW of the iron line should not be considered as an effective model selection tool.

As mentioned in Section 3.2, Fig. 4 clearly shows that both models give similar fluxes over the $\sim$0.1–40.0 keV band. The reflection model produces a Compton hump which peaks at $\sim$40 keV, while the transmission model predicts a steadily rising spectral shape above 20 keV. This implies that high-resolution X-ray spectroscopy in the hard-energy band may be required to tell which model provides a better interpretation to the data. If the spectrum is reflection dominated, the shape of the Compton hump should be detected. As the HXD/PIN failed to detect emission above 10 keV. the only current space mission which is likely to achieve this is *NuSTAR*.

Another way to examine the possibility of each model is to probe the origin of the neutral iron line. The 6.4 keV Fe Kα line could be fluorescent emission from (1) the accretion disc or (2) nearby low-ionization gas or molecular clouds. If the iron line is generated from disc reflection, it must come from the nucleus of the source, where an AGN is accommodated. The line is likely reflected from the edge of the cold outer disc as the torus. As for the latter possibility, a cooling flow can form clouds of atomic or molecular gas. Churazov et al. (1998) indicated that the cold clouds illuminated by the X-ray emission of the hot gas would lead to a 6.4 keV fluorescent line. O'Sullivan et al. (2012) show optical emission line filaments around the nucleus extended by a few arcsec, indicating that cold gas clouds are present.

In order to examine the hypotheses mentioned above, we generated *Chandra* spectra that exclude different sizes of central region and compared them with the *Chandra* 55 arcsec spectrum. We extracted a spectrum which excludes the central 2 arcsec radius circular region. which means an extraction from a 2–55 arcsec annulus source region. Another spectrum excluding the central 5 arcsec radius (5–55 arcsec annulus source region) was created using the same method. The background spectra were extracted using a 55–110 arcsec annulus, the same as the background region we used for the 55 arcsec spectrum extraction. We compare these spectra by plotting the line profiles in Fig. 6, and the red arrow indicates the 6.4 keV line in the rest frame. It can be seen that there is a lack of strong emission at 6.4 keV rest frame in the 2–55 arcsec and the 5–55 arcsec spectra. We tested the transmission model on these new spectra and found that the 6.4 keV Gaussian line is not strongly required. The normalization of the Gaussian component drops to a number close to zero. and the model works equally well if the Gaussian line is removed. This implies that most of the 6.4 keV emission is contributed by the very centre of the source, that is, the nucleus. The result cannot completely rule out the possibility that the 6.4 keV line originates from the cold clouds, but shows that the neutral iron line is more likely caused by the AGN. We hereby consider the reflection scenario to be the better interpretation to explain the X-ray spectrum of this source.

5 CONCLUSION

We carried out a *Suzaku* observation which offers simultaneous soft and hard X-ray band monitoring. During the observation. we avoided possible high-energy contamination from the nearby Type

2 AGN NGC 2785. Our result does not confirm the 3σ detection by the *BeppoSAX* PDS instrument. By analysing both the latest *Suzaku* and *Chandra* observations with long exposures, we found that the broad iron line shown in these spectra is in fact a combination of two components. Both the reflection and transmission models have been tested on our data sets. Statistically the data are consistent with either of the interpretations and both models behave very similarly from the low-energy band to ~40 keV. Nevertheless, both models indicate a Compton-thin absorber in this source. Assuming that IRAS 09104+4109 does not change significantly within a short time-scale, it is a Compton-thin AGN. Since the 6.4 keV Fe Kα seems to come from the central AGN, the reflection scenario is the better explanation to the source spectrum. However, the X-ray data below 10 keV give degenerate answers, and it is difficult to constrain the flux above 10 keV by current observations. We need high-spatial-resolution X-ray spectroscopy such as *NuSTAR* to detect the Compton hump predicted by the reflection model.

ACKNOWLEDGEMENTS

CYC and ACF thank J. Hlavacek-Larrondo and K. Iwasawa for useful discussions.

REFERENCES

Churazov E., Sunyaev R., Gilfanov M., Forman W., Jones C., 1998, MNRAS, 297, 1274
Comastri A., 2004, in Barger A. J., ed., Supermassive Black Holes in the Distant Universe, Vol. 308. Kluwer, Dordrecht, p. 245
Crawford C. S., Vanderriest C., 1996, MNRAS, 283, 1003
Fabian A. C., Crawford C. S., 1995, MNRAS, 274, L63
Fabian A. C. et al., 1994, ApJ, 436, L51
Franceschini A., Bassani L., Cappi M., Granato G. L., Malaguti G., Palazzi E., Persic M., 2000, A&A, 353, 910
Gandhi P., Horst H., Smette A., Hönig S., Comastri A., Gilli R., Vignali C., Duschl W., 2009, A&A, 502, 457
Hines D. C., Wills B. J., 1993, ApJ, 415, 82
Hlavacek-Larrondo J., Fabian A. C., Edge A. C., Ebeling H., Sanders J. S., Hogan M. T., Taylor G. B., 2012, MNRAS, 421, 1360
Iwasawa K., Fabian A. C., Ettori S., 2001, MNRAS, 321, L15
Kaastra J. S., 1992, http://www.sron.nl/files/HEA/SPEX/physics/megron.pdf
Kleinmann S. G., Hamilton D., Keel W. C., Wynn-Williams C. G., Eales S. A., Becklin E. E., Kuntz K. D., 1988, ApJ, 328, 161
Lanzuisi G., Piconcelli E., Fiore F., Feruglio C., Vignali C., Salvato M., Gruppioni C., 2009, A&A, 498, 67
Liedahl D. A., Osterheld A. L., Goldstein W. H., 1995, ApJ, 438, L115
Mewe R., Gronenschild E. H. B. M., van den Oord G. H. J., 1985, A&AS, 62, 197
Murphy E. M., Lockman F. J., Laor A., Elvis M., 1996, ApJS, 105, 369
O'Sullivan E. et al., 2012, MNRAS, 424, 2971
Piconcelli E., Fiore F., Nicastro F., Mathur S., Brusa M., Comastri A., Puccetti S., 2007, A&A, 473, 85
Ross R. R., Fabian A. C., 2005, MNRAS, 358, 211
Soifer B. T., Neugebauer G., Armus L., Shupe D. L., 1996, AJ, 111, 649
Tran H. D., Cohen M. H., Villar-Martin M., 2000, AJ, 120, 562
Vignali C. et al., 2011, MNRAS, 416, 2068

This paper has been typeset from a TEX/LATEX file prepared by the author.